Since January 2020 Elsevier has created a COVID-19 resource centre with free information in English and Mandarin on the novel coronavirus COVID-19. The COVID-19 resource centre is hosted on Elsevier Connect, the company's public news and information website.

Chemical Engineering Journal 430 (2022) 132723

Contents lists available at ScienceDirect

Chemical Engineering Journal

journal homepage: www.elsevier.com/locate/cej

Recycling respirator masks to a high-value product: From COVID-19 prevention to highly efficient battery separator

Soochan Kim [a,b], Xin Yang [c], Kaiwei Yang [a], He Guo [d], Misuk Cho [a], Young Jun Kim [a], Youngkwan Lee [a,*]

[a] School of Chemical Engineering, Sungkyunkwan University, Suwon 16419, Republic of Korea
[b] Department of Materials, University of Oxford, Oxford OX1 3PH, U.K
[c] Key Laboratory for Light-weight Materials, Nanjing Tech University, Nanjing 210009, China
[d] School of Advanced Materials Science & Engineering, Sungkyunkwan University, Suwon 16419, Republic of Korea

ARTICLE INFO

Keywords:
COVID-19
Recycling
Mask
Separator
Battery

ABSTRACT

COVID-19 is a pandemic that has caused serious disruption in almost every day-to-day life around the world, and wearing a mask is essential for human safety from this virus. However, masks are non-recyclable materials, and the accumulation of masks used every day causes serious environmental issues. In this study, we investigate the recycling of mask materials for addressing the environmental problems and transforming as a high value-added material through chemical modification of masks. The recycled mask is applied as a separator for aqueous rechargeable batteries, and shows outstanding safety and electrochemical performance than the existing separator. This approach will lead to an advanced energy technology considering nature after overcoming COVID-19.

1. Introduction

The COVID-19 pandemic has caused major disruptions to daily life globally, with more than 209 million infections (August 2021) and a steady rise in new cases [1]. Wearing masks (including respirators) indoors and outdoors is recommended as a personal preventive measure against COVID-19 [2]. The use of masks has increased rapidly, with more than 130 billion masks being discarded every month [3]. Recycling and separating the various components of masks is difficult; as a result, masks end up being incinerated or disposed in landfills, which leads to ecosystem disruption and environmental pollution [2,3]. Therefore, disposal of masks and residual materials is a major recent environmental issue.

Typically, the N95 grade (KF94; South Korea, KN95; China, DS/DLS2; Japan, FFP2; European Union) mask comprises multiple layers of Polypropylene (PP)-based nonwoven fabrics, where the most critical layer is the middle layer, which is produced by the melt-blown process [2]. The Middle filter layer (MF) comprises a three-dimensional (3D) network with a porosity of 90%, and it is highly hydrophobic, allowing it to effectively filter micro-level viral aerosols and dust [2,4]. Having a similar structure, three-dimensional porous polymeric films are considered promising in various fields such as energy, biological, and environmental applications, where they afford a large surface area [5,6]. The recycling of masks to exploit these advantages provides two-pronged benefits: environmental remediation and high value-added creation. Herein, we develop a high-value-added product by recycling masks used for COVID-19 prevention into highly efficient functional separators for aqueous rechargeable batteries (ARBs). As conventional separators, Glass fiber (GF)-based microporous separators have been widely used in most ARBs owing to their excellent wettability by aqueous electrolytes [7,8]. Nevertheless, the cost and thickness (~380 μm) of GF separators may impede their utility in commercial ARBs [7,8]. Therefore, finding an alternative to GF separators is urgent for the commercialization of ARBs. Thus, the MF is a promising candidate as a new alternative separator for ARBs, which can provide enhanced mechanical properties while being lightweight and allowing facile electrolyte transport, as well as affording a cost-effective and environmentally friendly processes through recycling masks.

2. Results and discussion

The proposed strategy for fabricating functional separators using recycled mask is presented in Fig. 1a. Through a simple reaction between PP and fuming sulfuric acid (FSA) [9], the hydrophobic surface of PP can be converted to hydrophilic with abundant –OH and –SO_3H groups within 10 min (see the supporting information for experimental

* Corresponding author.

https://doi.org/10.1016/j.cej.2021.132723
Received 27 June 2021; Received in revised form 20 August 2021; Accepted 25 September 2021
Available online 28 September 2021

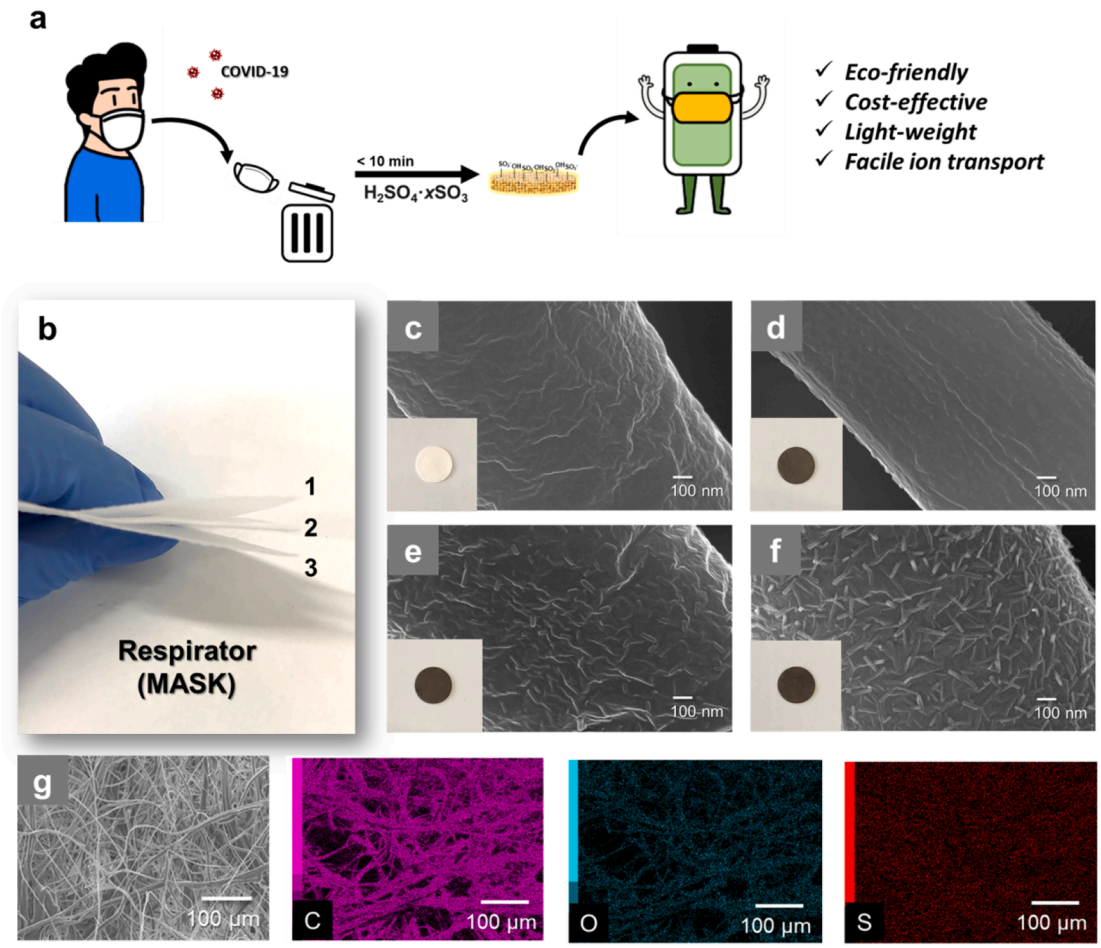

Fig. 1. a) Schematic of respirator (mask) recycling; b) optical image of three-layered mask; c) SEM image and optical image of pure Mask filter (MF), d-f) SEM image and optical image of sulfonated MFs (S-MF2, S-MF4, and S-MF6); g) EDS mapping of S-MF.

details). This process facilitates the conversion of discarded masks into high value-added products, while simultaneously removing the impurities in the masks. The structure of a mask consists of multiple layers (Fig. 1b). The MF consists of PP microfibers with a diameter of 1–10 μm and a thickness of approximately 140 μm (Fig. 1c and Fig. S1). After functionalization of MF with FSA, the color of the MF changed to light brown, and the fiber had a tough surface accroding to the FSA treatment time from 2 min to 6 min (Fig. 1d–f; S-MF2, S-MF4, and S-MF6). Rapid collapse of the surface and fiber was observed when FSA treatment was performed for more than 8 min (Fig. S2); thus, the appropriate time for surface treatment was set to < 8 min. The distribution of C, O, and S from energy dispersive spectroscopy (EDS) analysis (Fig. 1g and Fig. S3) further confirmed the uniform functionalization of the MF surface by FSA.

Detailed characterization of the structure and chemical features of the functionalized MF are shown in Fig. 2. MF functionalized by FSA (S-MF) has three types of chemical groups that can be transformed by sulfonic groups, according to previous studies. Abundant sulfonic groups can form metal–SO_3 complexes with metal ions, which can offer improved ion transport when used as a battery separator [10,11]. With increasing modification time of MF by FSA, the intensity of the specturms which presented –OH and –SO_3H groups increased based on the FT-IR spectra (Fig. 2b and Fig. S4). Pure MF presents the clear spectrum at 2954, 2915, 2871, 2839, 1451, 1374, 1165, and 1103 cm^{-1}, which are assigned to CH_3 stretching (2954 and 2871 cm^{-1}), CH_2 stretching (2915 and 2839 cm^{-1}), CH_2 and CH_3 bending (1451 cm^{-1}), CH_3 bending (1374 cm^{-1}), and C—C stretching (1165 and 1103 cm^{-1}). S-MF exhibited additional spetrum at 3419 cm^{-1}, broad peak near 1629 cm^{-1}, 1245 cm^{-1}, and 1057 cm^{-1}, which are assigned to O—H strectching, the vibration of C=C group, O=S=O asymmetric stretching, and O=S=O symmetric stretching [9,12–14].

Elemental analysis (Table S1) indicated increased formation of –SO_3H groups over the treatment time increased S content. From the increase S content, we could expected the SO_3H content of S-MFs (S-MF2: 5.1 %, S-MF4: 6.8 %, and S-MF6: 9.9%) The X-ray photoelectron spectra (XPS) of S-MF (Fig. 2c and Fig. S5) confirmed the appearance of peaks of S $2p_{1/2}$ (observed at 169.13 and 170.3 eV) and S $2p_{3/2}$ (at 168.52 eV). Moreover, the charateristic peaks at 168.52, 169.13, and 170.3 eV could assign to S=O, C—SO_3, and —C—SO_X (x = 2,3,4), respectively, which supports the assumed formation of surface SO_3H groups [15–17].

Thermogravimetric analysis (TGA) displayed a two-step degradation profile for the S-MFs (Fig. 2d), where the first weight loss (200–250 °C) was assigned to the degradation of SO_3H [18]. Upon increasing the SO_3H in the S-MFs, the first weight loss changed from ~96% to ~91%. Changes in the mechanical properties of MF according to the degree of modification are reflected in the stress-strain curves (Fig. 2e). First, the MF has robust properties compared to the blank GF (as a conventional separator). Upon increasing the MF modification time, the mechanical properties were slightly degraded. A sharp decrease in the mechanical properties was observed when FSA was treated for 6 min, related to increased surface defects. Moreover, after folding and twisting S-MF in 50 repeated cycles, the structure was stable without collapse and tear, unlike GF (Fig. S6). Thus, S-MF is expected to provide enhanced mechanical properties, compared with GF. As discussed earlier, the generation of SO_3H groups on the surface of MF increased the

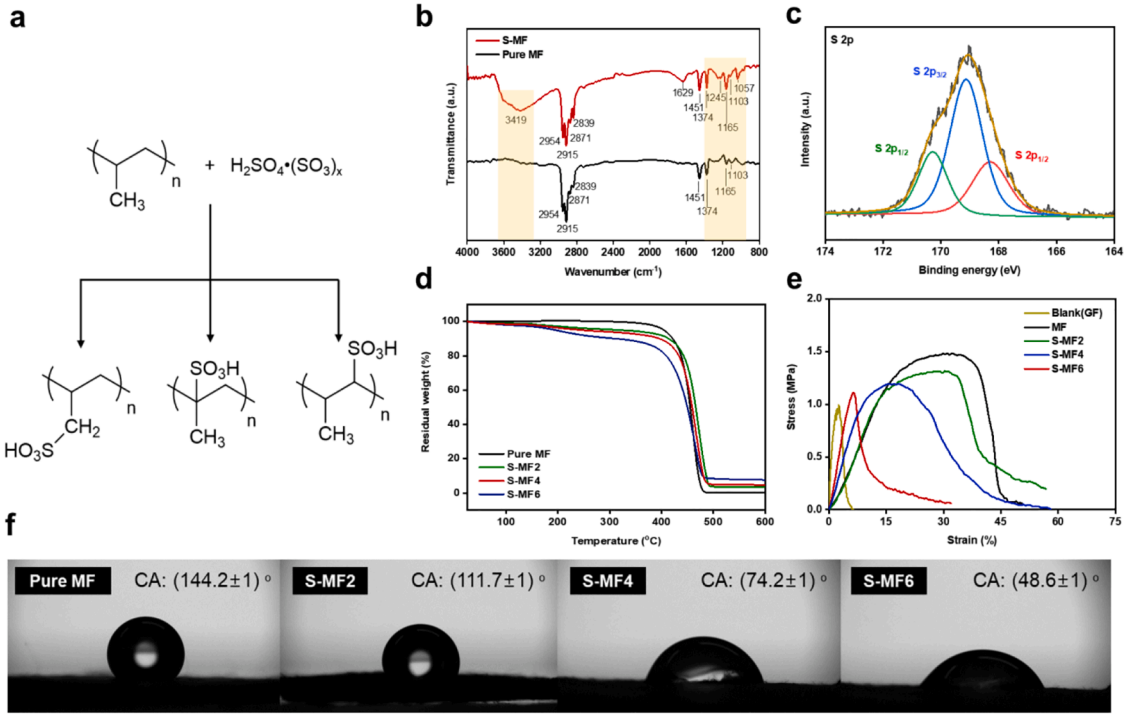

Fig. 2. a) Expected FSA process for polypropylene (PP), b) FT-IR spectra of pure MF and S-MF (S-MF6), c) XPS S 2p core level spectra of S-MF, d) TGA profiles of MF and S-MFs, e) stress-strain curves of blank glass fiber separator (GF), MF, and S-MFs, and e) digital photographs of contact angle of a 5 μL water drop on MF and S-MFs.

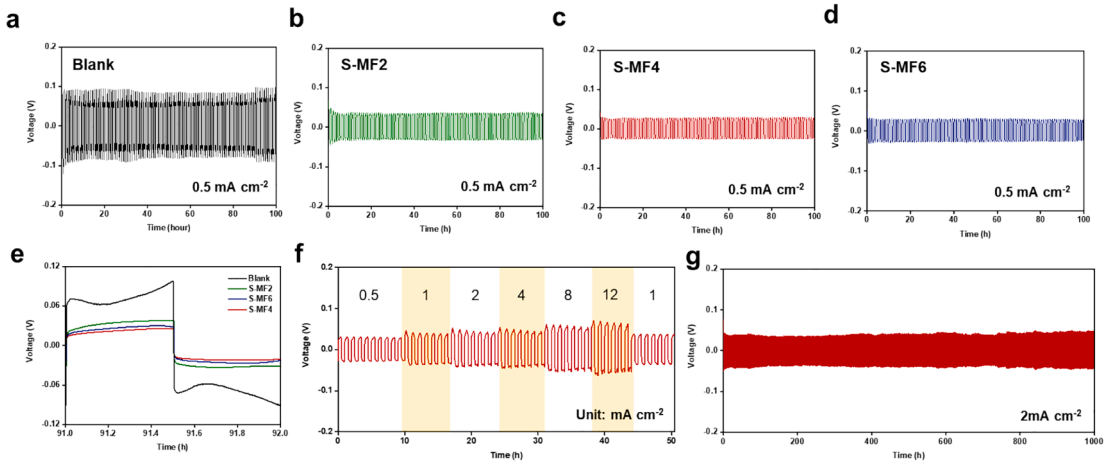

Fig. 3. a–d) Cycling performance of Zn//Zn symmetric cell with blank GF and S-MFs at current density of 0.5 mA cm^{-2} (for 0.25 mAh cm^{-2}); e) detailed voltage profiles obtained from Fig. 3a–d; f) cycling performance of Zn//Zn symmetric cell with optimized S-MF at current densities of 0.5–12 mA cm^{-2}; g) cycling performance of Zn//Zn symmetric cell with optimized S-MF at 2 mA cm^{-2} for 1000 h.

hydrophilicity, as confirmed by measuring the contact angles of the prepared S-MFs (Fig. 2f). The contact angles of GF exhibited in Fig. S7. The hydrophilicity of S-MF improved with increasing FSA treatment time. Therefore, considering these results (proper mechanical properties and hydrophilicity as a separator), 4 min is considered adequate for obtaining the optimized S-MF (S-MF4).

The developed S-MFs were used in the separator of aqueous Zn-ion batteries (ZIBs). ZIBs are considered the most promising candidates for large-scale energy storage systems because of their many advantages: abundant and cost-effective active materials, safe and stable working systems, high theoretical volumetric and gravimetric capacities of 5855 mA h cm^{-3} and 820 mA h g^{-1}, and eco-friendly fabrication process [19–21].

However, the growth of Zn dendrites on Zn anodes during battery cycling is a critical issue that must be addressed for the commercialization of ZIBs with efficient electrochemical system and safety battery.

As the separator for ZIBs, S-MF can provide a stable and electrochemically efficient battery system through mechanical suppression based on its 3D-structure, good electrolyte wettability, and facile ion transport owing to the abundant polar functional groups. To confirm the reactivity between Zn anode and S-MF separator, Zn anode was contacted for 24 h with wetted S-MF in 2 M $ZnSO_4$ aqueous solution. Through the XRD analysis, Zn anode remained the initial state without side reaction (Fig. S8).

The electrochemical behavior of the conventional GF (blank) and S-MF separator in a Zn//Zn symmetrical cell with 2 M $ZnSO_4$ aqueous

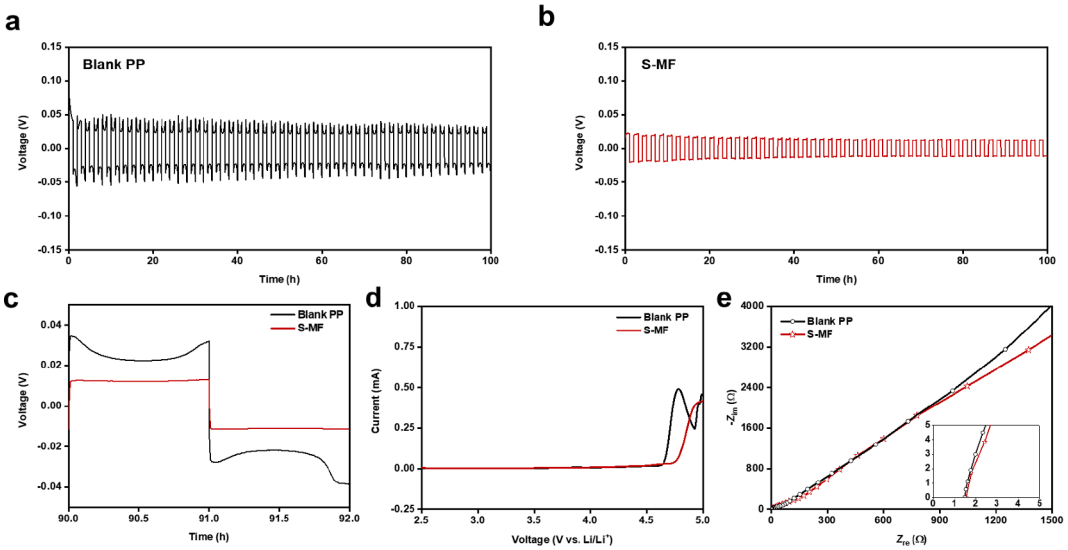

Fig. 4. a) and b) Cycling performance of Li//Li symmetric cell with blank PP and S-MF, respectively, at a current density at 0.5 mA cm^{-2} (for 0.5 mAh cm^{-2}); c) detailed voltage profiles from Fig. 4a and b; d) LSV curves of Li//separator//SS cells at scan rate of 0.1 mV s^{-1}; e) Nyquist plots of Li//separator//SS cells.

electrolyte is presented in Fig. 3a–d. At a current density of 0.5 mA cm^{-2} (0.25 mAh cm^{-2}), the over–potential of the blank cell was ~80 mV, whereas the over–potential of the S-MF symmetrical cells was lower, with a flat voltage plateau: 36 mV (S-MF2), 24 mV (S-MF4), and 30 mV (S-MF6). The low over–potential and flat voltage plateau indicate the reduced resistance in Zn nucleation and growth, which effectively improves the quality of the Zn plating and lowers the energy consumption [22]. The electrochemical impedance spectrum (EIS; Fig. S9) shows the low electrochemical resistance of the Zn symmetrical cell with S-MFs, indicating facile ion transport owing to the advantages of S-MFs. Among the symmetrical cells, that employing S-MF4 displayed superior electrochemical performance based on the suitable mechanical and ionic properties of S-MF4 (Fig. 2e and S8). Moreover, S-MF4 derived from other mask brand also presented similar electrochemical performance (Fig. S10). The structure of most MF is similar due to thea similar manufacturing process (melt-blown) under the required conditions (like as KF94, KN95, etc.). Detailed electrochemical evaluation of S-MF4 was undertaken by evaluating the rate performance at various current densities and the symmetrical cycling performance at 2 mA cm^{-2}. The symmetrical cell with S-MF4 showed stable voltage profiles with a low voltage hysteresis at high current densities (Fig. 3f). Upon increasing the current density from 0.5 to 12 mA cm^{-2}, the cell retained a stable voltage hysteresis without short-circuiting, and the voltage hysteresis recovered to the initial state at a current density of 0.5 mA cm^{-2} (Detailed voltage hysteresis in Fig. S11. Moreover, as shown in Fig. S12, Zn//Zn cell with conventional GF separator with increasing the current density from 0.5 to 12 mA cm^{-2}, the cell presented high voltage hysteresis, and the voltage hyteresis when the current density recovered to the initial current density of 0.5 mA cm^{-2} exhibited assymmetrical voltage profiles unlike symmetrical profiles of Fig. 3f. After 1000 h of battery cycling at 2 mA cm^{-2}, the S-MF4 cell showed a stable voltage profile with a relatively low voltage hysteresis of 41 mV, and stable Coulombic efficiency (Fig. 3g and Fig. S13). Moreover, after cycling, the S-MF and Zn metal anodes exhibited a stable morphology without structural collapse or serious deformations (Fig. S14). Thus, S-MF could deliver improved mechanical and electrochemical systems, leading to stable battery performance. As a modification of conventional PP based separator, an FSA-modified PP separator (S-PP) was prepared to confirm the effects of S-MF. Unlike S-MF, S-PP underwent rapid structural collapse and tearing despite the short modification time. When used as a separator for ZIBs, S-PP showed high electrochemical resistance and irregular cycling performance because of the low ion transport due to the pore size (Fig. S15 and S16). Thus, S-MF is more suitable as a separator for ARBs.

Fig. S17 presents the electrochemical performance of full cells comprising a Zn anode and MnO_2 cathode in a 2 M $ZnSO_4$ + 0.2 M $MnSO_4$ aqueous electrolyte, demonstrating its practical application. Fig. S17a shows the CV curves of the prepared Zn-MnO_2 cells with the blank (GF) and S-MF separator in the voltage range of 0.7–1.9 V (vs. Zn/Zn^{2+}) at a scan rate of 0.5 mVs^{-1}. Compared with the cell with the blank, the cell with S-MF displayed higher redox current densities and smaller polarization between the redox peaks, indicating an efficient electrochemical system. The cell with S-MF demonstrated good cycling stability (Fig. S17c), with 93.5% retention of the original specific capacity at 0.2 A g^{-1} after 200 cycles, owing to the improved electrochemical interface system. Meanwhile, the cell with the blank exhibited unstable performance with rapid specific capacity decay. From these results, it can predict the possibility of developing S-MF into combinations with various electrodes by applying it as a separator.

For further applications in conventional organic electrolyte systems, S-MF was evaluated as a separator for lithium-ion batteries (LIBs). LIBs are typical energy storage systems that operate in carbonate- or ether-based organic electrolytes [23–25].

Generally, a hydrophobic PP-based separator produced by the dry method is used with 25 μm thickness and a pore size of ~100 nm. To investigate the effect of S-MF on Li-metal anodes, galvanostatic cycling was carried out at 0.5 mA cm^{-2} in Li//Li symmetric cells with conventional PP and S-MF separators to observe the Li stripping/plating process in this system (Fig. 4a and 4b). The voltage profile of the symmetric cell with S-MF was smooth with a low voltage hysteresis throughout cycling, suggesting homogeneous current distribution at the Li metal surface [26,27]. As shown in Fig. 4c, stable voltage profiles of S-MF were observed, where the positive effects of S-MF on the LIB are derived from the porous structure of S-MF, robust mechanical properties, and facile ion transport through the interaction of Li^+ ions and SO_3^- groups on the S-MF surface. S-MF presented better electrochemical stability than the blank PP separator, as evaluated by LSV analysis at 0–5 V (vs. Li/Li^+) (Fig. 4d). The anodic potential window of the blank PP separator reached 4.6 V and that of S-MF reached 4.75 V. The electrochemical resistance of Li metal//separator//SS cells was measured by EIS (Fig. 4e), where the ion conductive characteristics of the cell with S-MF were similar to that with blank PP when the same electrolyte content, despite the thickness of the S-MF. Considering these characteristics, S-MF is expected to be highly utilized not only in aqueous electrolyte

systems, but also in organic electrolyte systems, and will further increase the value of recycling masks. In addition, to optimize for lithium ion batteries with organic electrolyte, reducing the thickness of S-MF like as conventional PP separators will be a necessary part of the next generation of researches, and as a suggestion of these studies, there may be development *via* cold-pressing for dense and thin separator and fabricating integral battery system including electrode, separator, and solid electrolyte.

3. Conclusion

In summary, a new approach for recycling masks to a high-value product, namely a highly efficient functional separator for rechargeable batteries, was developed. The discarded MF was converted to a valuable product through simple treatment using FSA within minutes. The recycled product presents better performance than conventional separators, emphasizing its importance. As a further advanced approach, recycling of MF *via* various chemical modifications is expected to be promising in numerous research fields (such as environmental catalyst, bio-engineering, energy-transforming), as well as separator for rechargeable batteries. From this approach, we will expand the research to produce more valuable products for human and nature.

CRediT authorship contribution statement

Soochan Kim:,**Xin Yang:**,**Kaiwei Yang:**,**He Guo:**,**Misuk Cho:**, **Young Jun Kim:**,**Youngkwan Lee:**.

Declaration of Competing Interest

The authors declare that they have no known competing financial interests or personal relationships that could have appeared to influence the work reported in this paper.

Acknowledgements

Dr. S. Kim and Dr. X. Yang contributed equally to this work. This work was supported by the Basic Science Research Program through the National Research Foundation of Korea (NRF) funded by the Ministry of Science and ICT (NRF-2019R1A2C1003594) and the Ministry of Education (NRF-2020R1A6A3A13074137).

Appendix A. Supplementary data

Supplementary data to this article can be found online at https://doi.org/10.1016/j.cej.2021.132723.

References

[1] V. Haldane, C. De Foo, S.M. Abdalla, A.-S. Jung, M. Tan, S. Wu, A. Chua, M. Verma, P. Shrestha, S. Singh, T. Perez, S.M. Tan, M. Bartos, S. Mabuchi, M. Bonk, C. McNab, G.K. Werner, R. Panjabi, A. Nordström, H. Legido-Quigley, Nat. Med. 27 (2021) 964.
[2] L. Liao, W. Xiao, M. Zhao, X. Yu, H. Wang, Q. Wang, S. Chu, Y. Cui, ACS Nano 14 (2020) 6348.
[3] M. Saberian, J. Li, S. Kilmartin-Lynch, M. Boroujeni, Sci. Total Environ. 769 (2021), 145527.
[4] J. Xu, X. Xiao, W. Zhang, R. Xu, S.C. Kim, Y. Cui, T.T. Howard, E. Wu, Y. Cui, One Earth 3 (2020) 574.
[5] Y. Zhao, B. Liu, L. Pan, G. Yu, Energy Environ. Sci. 6 (2013) 2856.
[6] S. Kim, M. Cho, Y. Lee, Adv. Energy Mater. 10 (2020) 1903477.
[7] J.H. Jo, C.-H. Jo, Z. Qiu, H. Yashiro, L. Shi, Z. Wang, S. Yuan, S.-T. Myung, Front. Chem. (2020) 8.
[8] Y. Qin, P. Liu, Q. Zhang, Q. Wang, D. Sun, Y. Tang, Y. Ren, H. Wang, Small 16 (2020) 2003106.
[9] M. Kaneko, H. Sato, Macromol. Chem. Phys. 206 (2005) 456.
[10] F. Yang, G. Xu, Y. Dou, B. Wang, H. Zhang, H. Wu, W. Zhou, J.-R. Li, B. Chen, Nat. Energy 2 (2017) 877.
[11] Y. Cao, H. Wu, G. Li, C. Liu, L. Cao, Y. Zhang, W. Bao, H. Wang, Y. Yao, S. Liu, F. Pan, Z. Jiang, J. Sun, Nano Lett. 21 (2021) 2997.
[12] J. Ihata, J. Polym. Sci. Polym. Chem. 26 (1988) 167.
[13] E. Wembabazi, P.J. Mugisha, A. Ratibu, D. Wendiro, J. Kyambadde, P.C. Vuzi, J. Spectrosc. (2015), 714396.
[14] C. Brun, M. Fromm, F. Berger, P. Delobelle, J. Takadoum, E. Beche, A. Chambaudet, F. Jaffiol, J. Polym. Sci. B Polym. Phys. 41 (2003) 1183.
[15] Y. Wang, D. Wang, M. Tan, B. Jiang, J. Zheng, N. Tsubaki, M. Wu, A.C.S. Appl Mater. Interfaces 7 (2015) 26767.
[16] J.F. Moulder, J. Chastain, R.C. King, *Handbook of X-ray photoelectron spectroscopy: a reference book of standard spectra for identification and interpretation of XPS data*, Physical Electronics (1995).
[17] X. Wen, Z. Zhao, S. Zhai, X. Wang, Y. Li, Diam. Relat. Mater. 105 (2020), 107791.
[18] M.M. Gomaa, C. Hugenschmidt, M. Dickmann, E.E. Abdel-Hady, H.F.M. Mohamed, M.O. Abdel-Hamed, Phys. Chem. Chem. Phys. 20 (2018) 28287.
[19] W. Du, E.H. Ang, Y. Yang, Y. Zhang, M. Ye, C.C. Li, Energy Environ. Sci. 13 (2020) 3330.
[20] Y. Zeng, X. Zhang, R. Qin, X. Liu, P. Fang, D. Zheng, Y. Tong, X. Lu, Adv. Mater. 31 (2019) 1903675.
[21] Y. An, Y. Tian, Y. Li, C. Wei, Y. Tao, Y. Liu, B. Xi, S. Xiong, J. Feng, Y. Qian, Chem. Eng. J. 400 (2020), 125843.
[22] Q. Zhang, J. Luan, L. Fu, S. Wu, Y. Tang, X. Ji, H. Wang, Angew. Chem. Int. Ed. 58 (2019) 15841.
[23] Y. Qian, C. Wei, Y. Tian, B. Xi, S. Xiong, J. Feng, Y. Qian, Chem. Eng. J. 421 (2021), 129685.
[24] S. Kim, D.H. Kim, M. Cho, W.B. Lee, Y. Lee, Small 16 (2020) 2004372.
[25] G. Yoo, S. Kim, C. Chanthad, M. Cho, Y. Lee, Chem. Eng. J. 405 (2021), 126628.
[26] S. Kim, J. Yang, D. Liu, Y. Huang, Y. Lee, Adv. Funct. Mater. 31 (2021) 2008354.
[27] S. Kim, D.H. Kim, M. Cho, W.B. Lee, Y. Lee, Chem. Eng. J. 420 (2021), 129772.